Three-dimensional analytical model for composite laminate with transverse cracks by assuming parabolic crack opening

Onodera, Sota
Department of Aeronautics and Astronautics, Kyushu University

Ryuzono, Kazuki
Department of Aeronautics and Astronautics, Kyushu University

Yashiro, Shigeki
Department of Aeronautics and Astronautics, Kyushu University

Okabe, Tomonaga
Department of Aerospace Engineering, Tohoku University

出版情報：Advanced Composite Materials. 32 (6), pp.866-888, 2023-01-16. Taylor and Francis
バージョン：
権利関係：

Three-Dimensional Analytical Model for Composite Laminate with Transverse Cracks by Assuming Parabolic Crack Opening

Sota Onodera[a]*, Kazuki Ryuzono[a], Shigeki Yashiro[a], Tomonaga Okabe[b,c,d]

[a]*Department of Aeronautics and Astronautics, Kyushu University, 744 Motooka, Nishi-ku, Fukuoka 819-0395, Japan;* [b]*Department of Aerospace Engineering, Tohoku University, 6-6-01, Aza-Aoba, Aramaki, Aobaku, Sendai, Miyagi, 980-8579, Japan;* [c]*Department of Materials Science and Engineering, University of Washington, BOX 352120, Seattle, WA 98195, USA;* [d]*Research Center for Structural Materials, Polymer Matrix Hybrid Composite Materials Group, National Institute for Materials Science, 1-2-1 Sengen, Tsukuba, Ibaraki, 305-0047, Japan*

Abstract

In this study, a model for the three-dimensional effective compliance of composite laminates with transverse cracks is developed based on continuum damage mechanics. Three-dimensional laminate theory is used to reproduce all the thermoelastic properties of the damaged laminate. The damage variable, which describes the degree of stiffness reduction caused by transverse cracking, is formulated based on a three-dimensional micromechanical model, with a loose boundary condition and assuming parabolic crack opening. These assumptions contribute to the analytical accuracy of the stiffness reduction model, while simplifying the damage variable expression. The effective thermomechanical properties of various composite laminates are predicted using the proposed model and compared with finite element analysis (FEA) and experimental results. We found that the proposed model with derived damage variable successfully reproduce the FEA and experimental results of stiffness degradation of damaged composite laminates.

Keywords: Continuum damage mechanics, Damage variable, Composite laminate, Stiffness degradation

*Corresponding author. Email: sota.onodera@aero.kyushu-u.ac.jp

1 Introduction

Carbon fiber-reinforced plastic (CFRP) and glass fiber-reinforced plastic (GFRP) laminates, which consist of unidirectional plies with various fiber angles, are widely used as the main components in primary structures owing to their excellent specific strength and rigidity. However, composite laminates exhibit nonlinear behaviors, owing due to transverse cracking, delamination, and fiber breakage.

Transverse cracking, which occurs parallel to the fibers in a ply, is typically the first damage mode. Transverse cracks cause a reduction in the laminate stiffness as well as crucial damage phenomena such as delamination and fiber breakage due to stress concentration at the crack tip. The mechanical behavior of composite laminates with transverse cracking must be evaluated during damage tolerance design. However, the stiffness reduction arising from transverse cracks varies depending on the material type, laminate layup, ply thickness, and fiber volume fraction. Therefore, it is inefficient to evaluate the effect of transverse cracks through experiments. Furthermore, in-plane and out-of-plane stiffness properties of the damaged laminate are required to evaluate the components under multiaxial loading. Therefore, an analytical model that effectively reproduces the stiffness reduction of various laminates is required.

Shear-lag analysis is commonly used to formulate the stiffness reduction and stress perturbation in cross-ply laminates with transverse cracks. Cox [1] first proposed this analysis method to evaluate the stress distribution around discontinuous fibers. Later, shear-lag analysis was used to approximate the stress distribution around transverse cracking in cross-ply laminates. Many one-dimensional [2–11] and two-dimensional [12–14] shear-lag models of cross-ply laminates have been established. One-dimensional shear-lag models differ only in their shear-lag parameters. Furthermore, two-dimensional models are almost equivalent to the one-dimensional models with a minor amendment to Poisson's effect.

Another method for modeling the stiffness degradation of damaged composite laminates is the variational approach. Hashin [15,16] first developed a variational model for stiffness reduction of cross-ply laminates with transverse cracking using the minimum complementary energy principle, while Lee et al. [17] formulated the minimum energy principle variational model for cross-ply laminates. In general, the minimum complementary energy principle results in a lower bound of the effective Young's modulus, whereas the minimum energy principle obtains the upper bound solution for Young's modulus. Hajikazemi [18,19] et al. and Vinogradov and Hashin [20,21] extend the variational model based on the minimum complementary energy principle to more general composite laminates.

Continuum damage mechanics (CDM) is an effective approach for treating diffused damage, such as transverse cracks. The origin of CDM is Kachanov's work on isotropic material creep damage [22]. Allen et al. [23] and Talreja [24] have both utilized CDM for orthotropic materials, namely, damaged

fiber-reinforced composite materials. CDM has good compatibility with laminate theory; therefore, CDM can treat composite laminates with various layups. The shear-lag analysis is difficult to formulate effective compliance of composite laminate with arbitrary layups. In the CDM, the damaged composite laminates with arbitrary layup sequences can be handled by simple formulae, and ordinary designers can use them easily. The variational analysis models are accurately reproduced the stress concentration of the crack tip and effective damaged laminate compliance, however, the formulated equations become complex. FEA can model transverse cracks explicitly and can accurately calculate stress concentrations at the crack tip. However, time and effort are required to generate a mesh around transverse cracks when the laminate configuration and transverse crack density change. In CDM, the effective stiffness/compliance is described as a function of the damage variable d $(0 \leq d \leq 1)$; therefore, the formulation of the damage variable is essential for developing the stiffness reduction model.

CDM is applied to reproduce the nonlinear behavior of cracked composite laminates using analytical [25,26] or finite element [27–29] models. In previous works [30–32], we formulated the damage variable associated with transverse cracks as a function of the transverse crack density (the number of cracks per laminate length) to clarify the physical meaning of the damage variable. Onodera and Okabe simplified the infinite series form of the damage variable in a previous study [30] by assuming a parabolic crack opening displacement to loosen the boundary condition of the governing differential equation. The derived damage variable is not only simpler than the complicated infinite series form but also successfully improves the two-dimensional analysis of the stiffness degradation of cracked composite laminates. However, this damage variable is obtained by two-dimensional micromechanical model [32,33]. In [31], the damage parameter ω is obtained by three-dimensional micromechanical model but this damage parameter has upper limit because of the small damage assumption [34]. Three-dimensional stiffness reduction model without such upper limit is required to represent nonlinear damage behavior of composite laminate subjected to out-of-plane or fatigue loading. Furthermore, the analytical model must be able to handle general composite laminates with arbitrary layups. However, those analytical models have seldom been formulated.

In this study, we analytically formulate a model of the three-dimensional effective compliance of composite laminates with transverse cracks by extending our previous two-dimensional model [32]. Three-dimensional laminate theory [35] is used to predict the in-plane and out-of-plane effective laminate elastic moduli. The three-dimensional effective compliance of the damaged ply proposed by Lopes et al. [36] is used to describe the stiffness reduction of the ply based on CDM. The damage variable, which describes the degree of stiffness reduction caused by transverse cracking, is derived from a three-dimensional micromechanics model by assuming a parabolic crack opening. Finally, we compare the stiffness reduction curves of the various laminates with our analytical results using finite element analysis (FEA) and the experimental results of previous studies.

2 Stiffness reduction model

2.1 Three-dimensional laminate theory

Three-dimensional theory [35] was used to calculate the effective compliance of a laminate with transverse cracks. As shown in Figure 1, the composite laminate was fabricated by stacking in the *Z*-direction. Coordinates (*X*, *Y*, *Z*) represent the laminate coordinate system. Stress and strain are described as follows:

$$\boldsymbol{\sigma} = \{\sigma_{XX} \quad \sigma_{YY} \quad \sigma_{ZZ} \quad \sigma_{YZ} \quad \sigma_{XZ} \quad \sigma_{XY}\}^{\mathrm{T}}, \tag{1}$$

$$\boldsymbol{\varepsilon} = \{\varepsilon_{XX} \quad \varepsilon_{YY} \quad \varepsilon_{ZZ} \quad \gamma_{YZ} \quad \gamma_{XZ} \quad \gamma_{XY}\}^{\mathrm{T}}. \tag{2}$$

The constitutive law is expressed by

$$\boldsymbol{\varepsilon} = \boldsymbol{S}\boldsymbol{\sigma} + \boldsymbol{\alpha}\Delta T, \tag{3}$$

where $\boldsymbol{S}$ is the compliance matrix, $\boldsymbol{\alpha}$ is the thermal expansion coefficient, and ΔT is the temperature difference from the stress-free temperature T_{sf} to the ambient temperature T. According to Gudmundson and Zang [35], the constitutive law of Eq. (3) is divided into in-plane and out-of-plane components, such that

$$\bar{\boldsymbol{\varepsilon}} = \bar{\boldsymbol{S}}\bar{\boldsymbol{\sigma}} + \bar{\boldsymbol{\alpha}}\Delta T, \tag{4}$$

where

$$\bar{\boldsymbol{\varepsilon}} = \boldsymbol{A}\boldsymbol{\varepsilon} = \begin{Bmatrix} \bar{\boldsymbol{\varepsilon}}_{\mathrm{I}} \\ \bar{\boldsymbol{\varepsilon}}_{\mathrm{O}} \end{Bmatrix} \text{ with } \bar{\boldsymbol{\varepsilon}}_{\mathrm{I}} = \begin{Bmatrix} \varepsilon_{XX} \\ \varepsilon_{YY} \\ \gamma_{XY} \end{Bmatrix} \text{ and } \bar{\boldsymbol{\varepsilon}}_{\mathrm{O}} = \begin{Bmatrix} \varepsilon_{ZZ} \\ \gamma_{XZ} \\ \gamma_{YZ} \end{Bmatrix}, \tag{5}$$

$$\bar{\boldsymbol{\sigma}} = \boldsymbol{A}\boldsymbol{\sigma} = \begin{Bmatrix} \bar{\boldsymbol{\sigma}}_{\mathrm{I}} \\ \bar{\boldsymbol{\sigma}}_{\mathrm{O}} \end{Bmatrix} \text{ with } \bar{\boldsymbol{\sigma}}_{\mathrm{I}} = \begin{Bmatrix} \sigma_{XX} \\ \sigma_{YY} \\ \sigma_{XY} \end{Bmatrix} \text{ and } \bar{\boldsymbol{\sigma}}_{\mathrm{O}} = \begin{Bmatrix} \sigma_{ZZ} \\ \sigma_{XZ} \\ \sigma_{YZ} \end{Bmatrix}, \tag{6}$$

$$\bar{\boldsymbol{S}} = \boldsymbol{A}\boldsymbol{S}\boldsymbol{A}^{\mathrm{T}} = \begin{bmatrix} \bar{\boldsymbol{S}}_{\mathrm{II}} & \bar{\boldsymbol{S}}_{\mathrm{IO}} \\ (\bar{\boldsymbol{S}}_{\mathrm{IO}})^{\mathrm{T}} & \bar{\boldsymbol{S}}_{\mathrm{OO}} \end{bmatrix}, \tag{7}$$

$$\bar{\boldsymbol{\alpha}} = \boldsymbol{A}\boldsymbol{\alpha} = \begin{Bmatrix} \bar{\boldsymbol{\alpha}}_{\mathrm{I}} \\ \bar{\boldsymbol{\alpha}}_{\mathrm{O}} \end{Bmatrix}. \tag{8}$$

The subscripts I and O denote the in-plane and out-of-plane components, respectively. $\boldsymbol{A}$ is a matrix that converts the stress and strain in Eqs. (1) and (2) into Eqs. (5) and (6), respectively. The conversion matrix $\boldsymbol{A}$ is as follows:

$$\boldsymbol{A} = \begin{bmatrix} 1 & 0 & 0 & 0 & 0 & 0 \\ 0 & 1 & 0 & 0 & 0 & 0 \\ 0 & 0 & 0 & 0 & 0 & 1 \\ 0 & 0 & 1 & 0 & 0 & 0 \\ 0 & 0 & 0 & 0 & 1 & 0 \\ 0 & 0 & 0 & 1 & 0 & 0 \end{bmatrix}. \tag{9}$$

In this study, we refer to the notations in Eqs. (4)–(8) as three-dimensional notation, whereas the notation in Eqs. (1)–(3) is referred to as normal notation.

Three-dimensional laminate theory assumes the following conditions.

$$\bar{\boldsymbol{\sigma}}^{\mathrm{L}} = \sum_{i=1}^{N} V_i \bar{\boldsymbol{\sigma}}^{i}, \tag{10}$$

$$\bar{\boldsymbol{\varepsilon}}^{\mathrm{L}} = \sum_{i=1}^{N} V_i \bar{\boldsymbol{\varepsilon}}^{i}, \tag{11}$$

$$\bar{\boldsymbol{\varepsilon}}_{\mathrm{I}}^{i} = \bar{\boldsymbol{\varepsilon}}_{\mathrm{I}}^{\mathrm{L}}, \tag{12}$$

$$\bar{\boldsymbol{\sigma}}_{\mathrm{O}}^{i} = \bar{\boldsymbol{\sigma}}_{\mathrm{O}}^{\mathrm{L}}. \tag{13}$$

The superscripts L and i denote the laminate and i-th ply, respectively. N is the number of plies and V_i is the volume fraction of the i-th ply in the laminate. Equation (12) represents the compatibility condition of the in-plane strains, and Eq. (13) is the equilibrium condition for out-of-plane stress. Under these conditions, the components of the laminate compliance $\bar{\boldsymbol{S}}^{\mathrm{L}}$ and effective thermal expansion coefficient $\bar{\boldsymbol{\alpha}}^{\mathrm{L}}$ in three-dimensional notation are obtained as follows:

$$\bar{\boldsymbol{S}}_{\mathrm{II}}^{\mathrm{L}} = \left[\sum_{i=1}^{N} V_i \left(\bar{\boldsymbol{S}}_{\mathrm{II}}^{i}\right)^{-1}\right]^{-1}, \tag{13}$$

$$\bar{\boldsymbol{S}}_{\mathrm{IO}}^{\mathrm{L}} = \bar{\boldsymbol{S}}_{\mathrm{II}}^{\mathrm{L}} \left[\sum_{i=1}^{N} V_i \left(\bar{\boldsymbol{S}}_{\mathrm{II}}^{i}\right)^{-1} \bar{\boldsymbol{S}}_{\mathrm{IO}}^{i}\right], \tag{14}$$

$$\bar{\boldsymbol{S}}_{\mathrm{OO}}^{\mathrm{L}} = \left(\bar{\boldsymbol{S}}_{\mathrm{IO}}^{\mathrm{L}}\right)^{\mathrm{T}} \left(\bar{\boldsymbol{S}}_{\mathrm{II}}^{\mathrm{L}}\right)^{-1} \bar{\boldsymbol{S}}_{\mathrm{IO}}^{\mathrm{L}} + \sum_{i=1}^{N} V_i \left[\bar{\boldsymbol{S}}_{\mathrm{OO}}^{i} - \left(\bar{\boldsymbol{S}}_{\mathrm{IO}}^{i}\right)^{\mathrm{T}} \left(\bar{\boldsymbol{S}}_{\mathrm{II}}^{i}\right)^{-1} \bar{\boldsymbol{S}}_{\mathrm{IO}}^{i}\right], \tag{15}$$

$$\bar{\boldsymbol{\alpha}}_{\mathrm{I}}^{\mathrm{L}} = \bar{\boldsymbol{S}}_{\mathrm{II}}^{\mathrm{L}} \left[\sum_{i=1}^{N} V_i \left(\bar{S}_{\mathrm{II}}^{i}\right)^{-1} \bar{\boldsymbol{\alpha}}_{\mathrm{I}}^{i}\right], \tag{16}$$

$$\bar{\boldsymbol{\alpha}}_{\mathrm{O}} = \left(\bar{\boldsymbol{S}}_{\mathrm{IO}}^{\mathrm{L}}\right)^{\mathrm{T}} \left(\bar{\boldsymbol{S}}_{\mathrm{II}}^{\mathrm{L}}\right)^{-1} \bar{\boldsymbol{\alpha}}_{\mathrm{I}}^{\mathrm{L}} + \sum_{i=1}^{N} V_i \left[\bar{\boldsymbol{\alpha}}_{\mathrm{O}}^{i} - \left(\bar{\boldsymbol{S}}_{\mathrm{IO}}^{i}\right)^{\mathrm{T}} \left(\bar{\boldsymbol{S}}_{\mathrm{II}}^{i}\right)^{-1} \bar{\boldsymbol{\alpha}}_{\mathrm{I}}^{i}\right]. \tag{17}$$

Given the effective compliance $\boldsymbol{S}^{i}$ and thermal expansion coefficient $\boldsymbol{\alpha}^{i}$ of the i-th ply in the normal notation, their counterparts in the three-dimensional notation can be calculated using Eqs. (7) and (8), respectively. The effective laminate compliance $\bar{\boldsymbol{S}}^{\mathrm{L}}$ and effective thermal expansion coefficient $\bar{\boldsymbol{\alpha}}^{\mathrm{L}}$ in three-dimensional notation can be obtained using Eqs. (13)-(17). Then, $\bar{\boldsymbol{S}}^{\mathrm{L}}$ and $\bar{\boldsymbol{\alpha}}^{\mathrm{L}}$ are converted into $\boldsymbol{S}^{\mathrm{L}} = \{S_{ij}^{\mathrm{L}}\}$ and $\boldsymbol{\alpha}^{\mathrm{L}} = \{\alpha_{i}^{\mathrm{L}}\}$ in the normal notation to obtain the thermo-mechanical properties of the cracked laminate. Thus, the thermomechanical properties of the laminate can be obtained:

$$E_X^{\mathrm{L}} = \frac{1}{S_{11}^{\mathrm{L}}}, E_Y^{\mathrm{L}} = \frac{1}{S_{22}^{\mathrm{L}}}, E_Z^{\mathrm{L}} = \frac{1}{S_{33}^{\mathrm{L}}}, \tag{18}$$

$$G_{YZ}^{\mathrm{L}} = \frac{1}{S_{44}^{\mathrm{L}}}, G_{XZ}^{\mathrm{L}} = \frac{1}{S_{55}^{\mathrm{L}}}, G_{XY}^{\mathrm{L}} = \frac{1}{S_{66}^{\mathrm{L}}}, \tag{19}$$

$$\nu_{YZ}^{\mathrm{L}} = -\frac{S_{23}^{\mathrm{L}}}{S_{22}^{\mathrm{L}}}, \nu_{XZ}^{\mathrm{L}} = -\frac{S_{13}^{\mathrm{L}}}{S_{11}^{L}}, \nu_{XY}^{\mathrm{L}} = -\frac{S_{12}^{\mathrm{L}}}{S_{11}^{\mathrm{L}}}, \tag{20}$$

$$\alpha_X^{\mathrm{L}} = \alpha_1^{\mathrm{L}}, \alpha_Y^{\mathrm{L}} = \alpha_2^{\mathrm{L}}, \alpha_Z^{\mathrm{L}} = \alpha_3^{\mathrm{L}}, \alpha_{YZ}^{\mathrm{L}} = \alpha_4^{\mathrm{L}}, \alpha_{XZ}^{\mathrm{L}} = \alpha_5^{\mathrm{L}}, \alpha_{XY}^{\mathrm{L}} = \alpha_6^{\mathrm{L}}, \tag{21}$$

where E is Young's modulus, G is the shear modulus, ν is Poisson's ratio, and α is the thermal expansion coefficient. The subscripts X, Y, and Z indicate the laminate coordinate-directions.

2.2 Effective compliance of damaged ply

The three-dimensional effective compliance proposed by Lopes et al. [36] was used to describe the ply with transverse cracks, as shown in Figure 2 (a). The material coordinates are defined as (1,2,3), where "1" is the fiber direction, "2" is the transverse direction, and "3" is the through-thickness direction. The origin of the material coordinate system is placed at the center of the ply. In the material coordinate system, the effective compliance for orthotropic damaged ply of the Lopes model is described as follows:

$$\boldsymbol{S}_{\mathrm{mat}} = \begin{bmatrix} \frac{1}{(1-d_1)E_1} & -\frac{\nu_{12}}{E_1} & -\frac{\nu_{12}}{E_1} & 0 & 0 & 0 \\ & \frac{1}{(1-d_2)E_2} & -\frac{\nu_{23}}{E_2} & 0 & 0 & 0 \\ & & \frac{1}{(1-d_3)E_2} & 0 & 0 & 0 \\ & & & \frac{1}{(1-d_4)G_{23}} & 0 & 0 \\ & & & & \frac{1}{(1-d_5)G_{12}} & 0 \\ & \text{sym.} & & & & \frac{1}{(1-d_6)G_{12}} \end{bmatrix} \tag{22}$$

d_i is the damage variable. The thermal expansion coefficient of the ply in the material coordinate system is expressed as

$$\boldsymbol{\alpha}_{\mathrm{mat}} = \{\alpha_1 \quad \alpha_2 \quad \alpha_2 \quad 0 \quad 0 \quad 0\} \tag{23}$$

The effective compliance $\boldsymbol{S}^i$ and thermal expansion coefficient $\boldsymbol{\alpha}^i$ of the i-th ply in the laminate coordinate system were obtained by rotating the fiber orientation.

$$\boldsymbol{S}^i = \boldsymbol{R}(\theta^i)\boldsymbol{S}_{\mathrm{mat}}\boldsymbol{T}(-\theta^i), \tag{24}$$

$$\boldsymbol{\alpha}^i = \boldsymbol{R}(\theta^i)\boldsymbol{\alpha}_{\mathrm{mat}}, \tag{25}$$

θ^i is fiber angle of the i-th ply. $\boldsymbol{T}(\theta^i)$ and $\boldsymbol{R}(\theta^i)$ are the coordinate conversion matrices of the stress and strain, respectively, defined by

$$\boldsymbol{T}(\theta^i) = \begin{bmatrix} \cos^2\theta^i & \sin^2\theta^i & 0 & 0 & 0 & -\sin 2\theta^i \\ \sin^2\theta^i & \cos^2\theta^i & 0 & 0 & 0 & \sin 2\theta^i \\ 0 & 0 & 1 & 0 & 0 & 0 \\ 0 & 0 & 0 & \cos\theta^i & \sin\theta^i & 0 \\ 0 & 0 & 0 & -\sin\theta^i & \cos\theta^i & 0 \\ \sin\theta^i\cos\theta^i & -\sin\theta^i\cos\theta^i & 0 & 0 & 0 & \cos 2\theta^i \end{bmatrix}, \tag{26}$$

$$\boldsymbol{R}(\theta^i) = \begin{bmatrix} \cos^2\theta^i & \sin^2\theta^i & 0 & 0 & 0 & -\sin\theta^i\cos\theta^i \\ \sin^2\theta^i & \cos^2\theta^i & 0 & 0 & 0 & \sin\theta^i\cos\theta^i \\ 0 & 0 & 1 & 0 & 0 & 0 \\ 0 & 0 & 0 & \cos\theta^i & \sin\theta^i & 0 \\ 0 & 0 & 0 & -\sin\theta^i & \cos\theta^i & 0 \\ \sin 2\theta^i & -\sin 2\theta^i & 0 & 0 & 0 & \cos 2\theta^i \end{bmatrix}. \quad (26)$$

Once the damage variables are formulated, the effective compliance and thermal expansion coefficient can be obtained using Eqs. (24) and (25), respectively. The formulation of the damage variables is discussed in the next section.

2.3 Formulation of damage variable assuming parabolic crack opening

The damage variables d_2 and d_6 were derived from a three-dimensional micromechanics model by assuming a parabolic crack opening of transverse cracks. As shown in Figure 2 (b), the representative volume element (RVE) of the damaged ply was considered. Coordinates (x, y, z) represent the RVE coordinate system. The origin of the RVE coordinate system is set at the center of RVE, and the origin positions between the material and RVE coordinate systems do not necessarily coincide. The length, width, and thickness of the RVE were $2l$, $2h$, and $2t$, respectively, where $2l$ is the transverse crack spacing, $2h$ is the ply width, and $2t$ is the ply thickness. Both sides of the RVE were cracked surfaces. The RVE is symmetric, and the defined analysis domain is the quarter of RVE: $0 \le x \le t$, $0 \le y \le l$, and $0 \le z \le h$.

The strain–stress relationship of transversely isotropic material in the RVE was described as follows.

$$\varepsilon_x = \frac{\partial u}{\partial x} = \frac{1}{E_2}\sigma_x - \frac{\nu_{23}}{E_2}\sigma_y - \frac{\nu_{21}}{E_2}\sigma_z \quad (27)$$

$$\varepsilon_y = \frac{\partial v}{\partial y} = -\frac{\nu_{23}}{E_2}\sigma_x + \frac{1}{E_2}\sigma_y - \frac{\nu_{21}}{E_2}\sigma_z \quad (28)$$

$$\varepsilon_z = \frac{\partial w}{\partial z} = -\frac{\nu_{21}}{E_2}\sigma_x - \frac{\nu_{21}}{E_2}\sigma_y + \frac{1}{E_1}\sigma_z \quad (29)$$

$$\gamma_{xy} = \frac{\sigma_{xy}}{G_{23}} = \frac{\partial v}{\partial x} + \frac{\partial u}{\partial y} \cong \frac{\partial v}{\partial x} \quad (30)$$

$$\gamma_{xz} = \frac{\sigma_{xz}}{G_{12}} = \frac{\partial u}{\partial z} + \frac{\partial w}{\partial x} \cong 0 \quad (31)$$

$$\gamma_{yz} = \frac{\sigma_{yz}}{G_{12}} = \frac{\partial v}{\partial z} + \frac{\partial w}{\partial y} \cong \frac{\partial v}{\partial z} \quad (32)$$

The subscripts x, y, and z denote the RVE coordinate directions; u, v, and w are the displacements along the x-, y-, and z-axes, respectively. We assumed that $\partial u/\partial y \ll \partial v/\partial x$, $\partial w/\partial y \ll \partial v/\partial z$ and $\gamma_{xz} \ll 1$ in Eqs. (30)-(32). Following our previous study [31], the relationship between ε_x, ε_y, and ε_z was assumed as follows:

$$\varepsilon_x(x,y,z) = a\varepsilon_y(x,y,z), \tag{33}$$

$$\varepsilon_z(x,y,z) = b\varepsilon_y(x,y,z). \tag{34}$$

Constant parameters a and b are the average Poisson's ratios and are determined by equilibrium equations. From Eqs. (27)–(34), the stresses were expressed as functions of the partial differentiation of v, as follows.

$$\sigma_x = E_2 \frac{\nu_{23} + \nu_{12}\nu_{21} + (1-\nu_{12}\nu_{21})a + \nu_{12}(1+\nu_{23})b}{(1+\nu_{23})(1-\nu_{23}-2\nu_{12}\nu_{21})} \frac{\partial v}{\partial y} \tag{35}$$

$$\sigma_y = E_2 \frac{1 - \nu_{12}\nu_{21} + (\nu_{23} + \nu_{12}\nu_{21})a + \nu_{12}(1+\nu_{23})b}{(1+\nu_{23})(1-\nu_{23}-2\nu_{12}\nu_{21})} \frac{\partial v}{\partial y} \tag{36}$$

$$\sigma_z = E_1 \frac{\nu_{21} + \nu_{21}a + (1-\nu_{23})b}{1-\nu_{23}-2\nu_{12}\nu_{21}} \frac{\partial v}{\partial y} \tag{37}$$

$$\sigma_{xy} = G_{23} \frac{\partial v}{\partial x} \tag{38}$$

$$\sigma_{xz} = 0 \tag{39}$$

$$\sigma_{yz} = G_{12} \frac{\partial v}{\partial z} \tag{40}$$

σ_{xz} is always zero by assuming $\gamma_{xz} \cong 0$ in Eq. (31). The three-dimensional equilibrium equation without the body force was expressed as follows.

$$\frac{\partial \sigma_x}{\partial x} + \frac{\partial \sigma_{xy}}{\partial y} + \frac{\partial \sigma_{xz}}{\partial z} = 0 \tag{41}$$

$$\frac{\partial \sigma_{xy}}{\partial x} + \frac{\partial \sigma_y}{\partial y} + \frac{\partial \sigma_{yz}}{\partial z} = 0 \tag{42}$$

$$\frac{\partial \sigma_{xz}}{\partial x} + \frac{\partial \sigma_{yz}}{\partial y} + \frac{\partial \sigma_z}{\partial z} = 0 \tag{43}$$

Substituting Eqs. (35)–(40) into Eqs. (41)–(43), the following average Poisson's ratio and Laplace equation for v were obtained:

$$a = -\left(\nu_{23} + \frac{G_{23}}{E_2}(1-\nu_{23}^2) - \frac{G_{12}}{E_1}\nu_{12}(1+\nu_{23})\right), \tag{44}$$

$$b = -\left(\nu_{21} - \frac{G_{23}}{E_2}\nu_{21}(1+\nu_{23}) + \frac{G_{12}}{E_1}(1-\nu_{12}\nu_{21})\right), \tag{45}$$

$$\frac{\partial^2 v}{\partial x^2} + \lambda_1^2 \frac{\partial^2 v}{\partial y^2} + \lambda_2^2 \frac{\partial^2 v}{\partial z^2} = 0, \tag{46}$$

where

$$\lambda_1 = \sqrt{\frac{E_2}{G_{23}} \frac{1 - \nu_{12}\nu_{21} + (\nu_{12}\nu_{21} + \nu_{23})a + \nu_{12}(1+\nu_{23})b}{(1+\nu_{23})(1-\nu_{23}-2\nu_{12}\nu_{21})}}, \tag{47}$$

$$\lambda_2 = \sqrt{\frac{G_{12}}{G_{23}}}. \tag{48}$$

The boundary conditions considered for the Laplace equation of v were as follows.

$$v = 0 \text{ on the surface } y = 0 \tag{49}$$

$$\frac{\partial v}{\partial y} = 0 \text{ on the surface } y = l \tag{50}$$

$$\frac{\partial v}{\partial x} = 0 \text{ on the surface } x = 0 \tag{51}$$

$$\frac{\partial v}{\partial z} = 0 \text{ on the surface } z = h \tag{52}$$

$$\frac{\partial v}{\partial z} = 0 \text{ on the surface } z = 0 \tag{53}$$

$$v = \varepsilon_y^{\infty} y \text{ on the surface } x = t \tag{54}$$

The reference position of the displacement v is defined in Eq. (49). Eq. (50) represents the traction-free condition on the crack surface. Eq. (51) indicates that $\sigma_{xy} = 0$; Eqs. (52) and (53) were obtained from $\sigma_{yz} = 0$. Based on previous studies [17,30], we assumed that the whole neighboring plies of the cracked ply are rigid in Eq. (54). In other words, the displacement v at the interfaces of the cracked ply was deformed by the uniform ply strain ε_y^{∞} along the y-direction, regardless of the transverse crack. Using the variable separation method in Laplace equation (46) under boundary conditions (49)–(54), the infinite series form of the displacement v was obtained as follows:

$$v = \frac{8l}{\pi^2}\left[\sum_{n=1}^{\infty} \frac{(-1)^{n+1}}{(2n-1)^2} \frac{\cosh[(2n-1)\pi\lambda_1 x/(2l)]}{\cosh[(2n-1)\pi\lambda_1 t/(2l)]} \sin\left(\frac{2n-1}{2l}\pi y\right)\right]\varepsilon_y^{\infty}. \tag{55}$$

Although Eq. (55) is a solution, it is quite complicated. To simplify the solution and loosen the boundary condition, we assumed the following parabolic displacement form:

$$v(x, y, z) = D(z)\big(A(y)x^2 + B(y)x + C(y)\big) \text{ with } D(z) \neq 0. \tag{56}$$

Here, $A(y)$, $B(y)$, $C(y)$, and $D(z)$ are arbitrary functions that satisfy the boundary conditions. Substituting Eq. (56) into Eqs. (51) and (54), we obtained:

$$B(y) = 0, \tag{57}$$

$$D(z)C(y) = \varepsilon_y^{\infty} y - D(z)A(y)t^2. \tag{58}$$

Using Eqs. (57) and (58), Eq. (56) was rewritten as

$$v = D(z)A(y)(x^2 - t^2) + \varepsilon_y^{\infty} y. \tag{59}$$

Substituting Eq. (59) into Eqs. (49), (50), (52), and (53), the following equations were obtained.

$$A(0) = 0 \tag{60}$$

$$D(z)\frac{dA}{dy}(l) \cdot (x^2 - t^2) + \varepsilon_y^{\infty} = 0 \tag{61}$$

$$\frac{dD}{dz}(h) = 0 \tag{62}$$

$$\frac{dD}{dz}(0) = 0 \tag{63}$$

From Eq. (58), the following equation was obtained.

$$D(z)\left(C(y) + A(y)t^2\right) = \varepsilon_y^{\infty} y \tag{64}$$

By comparing the left- and right-hand sides of the above equation, the $D(z)$ can be determined as follows.

$$D(z) = 1\ (= \text{Const.}) \tag{65}$$

Since $D(z)$ is constant, the displacement v is constant in the thickness direction. Eq. (65) obviously satisfied Eqs. (62) and (63). Using Eqs. (59) and (64), the Laplace equation (46) was rewritten as

$$2A(y) + \lambda_1^2 \frac{d^2A}{dy^2}(x^2 - t^2) = 0. \tag{66}$$

From Eq. (65), $A(y) = 0$ was obtained. However, the boundary condition of Eq. (61) could not be satisfied. To clear this roadblock, Eqs. (46) and (50) were averaged across the x-direction [37].

$$\frac{1}{t}\int_0^t \frac{\partial v}{\partial y} dx \bigg|_{y=l} = 0 \tag{67}$$

$$\frac{1}{t}\int_0^t \left(\frac{\partial^2 v}{\partial x^2} + \lambda_1^2 \frac{\partial^2 v}{\partial y^2} + \lambda_2^2 \frac{\partial^2 v}{\partial z^2}\right) dx = 0 \tag{68}$$

Eqs. (67) and (68) considering the loose boundary condition implies that the boundary condition (Eq. (50)) and governing equation (Eq. (46)) are averaged over the thickness direction following McCartney [37]. Therefore, Eqs. (67) and (68) are not exact expressions but approximate equations following Ref. [37]. In the process of deriving damage variable d_2, the displacement v is averaged over x and z-direction to derive the inelastic strain, so the effect of this approximation is small. By substituting Eqs. (59) and (64), Eqs. (66) and (67) were rewritten as

$$\frac{dA}{dy}(l) = \frac{3\varepsilon_y^{\infty}}{2t^2}, \text{and} \tag{69}$$

$$\frac{d^2A}{dy^2}(y) - \beta_{3D}^2 A(y) = 0, \tag{70}$$

where

$$\beta_{3D} = \frac{\sqrt{3}}{\lambda_1 t} \tag{71}$$

Under the boundary conditions in Eqs. (60) and (68), the ordinary 2nd order differential equation in Eq. (69) could be solved.

$$A(y) = \frac{3\varepsilon_y^{\infty}}{2t^2\beta_{3D}} \frac{\sinh \beta_{3D} y}{\cosh \beta_{3D} l} \tag{72}$$

The displacement v was obtained using Eqs. (59), (64), and (71).

$$v = \frac{3\varepsilon_y^{\infty}}{2t^2\beta_{3D}} \frac{\sinh \beta_{3D} y}{\cosh \beta_{3D} l}(x^2 - t^2) + \varepsilon_y^{\infty} y \tag{73}$$

The parabolic form of v (Eq. (72)) is simpler than that in the infinite form (Eq. (55)). According to our previous paper [30], the damage variable d_2 is the ratio of the inelastic strain due to crack opening to the ply strain ε_y^{∞}; therefore, d_2 was formulated using Eq. (72).

$$d_2 = \frac{1}{\varepsilon_y^{\infty}}\left(\varepsilon_y^{\infty} - \frac{1}{lth}\int_0^h \int_0^t v(x, l, z)dx\, dz\right) = \frac{2\rho}{\beta_{3D}} \tanh \frac{\beta_{3D}}{2\rho} \text{ (Parabolic Solution)} \tag{74}$$

where $\rho = 1/(2l)$ is the transverse crack density. Eq. (73) refers to the parabolic solution used in this study; the infinite form of the damage variable d_2 was derived using Eq. (55) [31]:

$$d_2 = 1 - \frac{8}{\pi^3 \lambda_1 t} \sum_{n=1}^{\infty} \frac{1}{(2n-1)^3} \frac{\tanh[(2n-1)\pi\lambda_1 t\rho]}{\rho} \text{ (Infinite Series Solution).} \tag{75}$$

The parabolic solution of d_2 (Eq.(73)) is much simplified compared with that of the infinite series solution (Eq.(74)). These two solutions are compared in detail later.

The damage variable d_6 was formulated from three-dimensional micromechanics model developed in our previous studies [31,32]. The parabolic and infinite solutions of d_6 were expressed as follows:

$$d_6 = \frac{2\rho}{\beta_{12}} \tanh \frac{\beta_{12}}{2\rho} \text{ (Parabolic solution),} \tag{76}$$

$$d_6 = 1 - \frac{8}{\pi^3 t} \sum_{n=1}^{\infty} \frac{1}{(2n-1)^3} \frac{\tanh[(2n-1)\pi t\rho]}{\rho} \text{ (Infinite series solution).} \tag{77}$$

The remaining damage variables were d_1, d_3, d_4, and d_5. The ply has transverse cracks only; therefore, d_1 and d_3 were postulated as follows:

$$d_1 = 0, d_3 = 0. \tag{78}$$

The shear damage variables d_4 and d_5 were calculated using the following approximate expressions [38]:

$$\frac{1}{1-d_4} = \frac{1}{2}\left(\frac{1}{1-d_2} + \frac{1}{1-d_3}\right), \quad \frac{1}{1-d_5} = \frac{1}{2}\left(\frac{1}{1-d_1} + \frac{1}{1-d_3}\right). \tag{79}$$

3 Results and discussion

The effective thermoelastic properties of CFRP and GFRP composite laminates with various layups were predicted by the three-dimensional stiffness reduction model presented in the previous section. The predicted results were compared with the FEA and experimental results from previous studies to validate the proposed model. The material properties used for validation are listed in Table 1.

3.1 Cross-ply laminate

In the calculation of the effective properties of the cross-ply laminate, the stiffness reduction model with parabolic solutions of the damage variables (Eqs. (73) and (75)) are compared with those of the more complicated model with infinite series (Eqs. (74) and (76)) and National Physical Laboratory (NPL) models [39,40]. The NPL model is the generalized plane strain model that satisfy the equilibrium and compatibility equations. Therefore, the NPL model is exact solution, and the stress perturbation along the interfaces of the cracked ply is considered. Our proposed model is the approximate solution that does not satisfy the compatibility equation because of Eqs. (33) and (34). Furthermore, the stress distribution along the interfaces of the cracked ply in our model is constant due to Eq. (54), regardless of transverse cracking. To verify our model, the present model is compared with the NPL model that is exact solution. The effective Young's moduli of the $[0/90_2]_s$, $[0/90_2/0]_s$, and $[0/90/0/90]_s$ CFRP laminates and the crack opening displacement of a transverse crack in the $[0/90]_s$ CFRP laminate were predicted. The material parameters of CFRP1 were used in the calculation, as summarized in Table 1.

Figure 3 shows the nominal axial Young's modulus of cross-ply laminates with a ply thickness of 0.127 mm as a function of the transverse crack density. Compared with the infinite series solution, the present model with a parabolic solution of the damage variables is in good agreement with the NPL model results. Figure 4 shows the crack opening displacement of a transverse crack in the $[0/90]_s$ CFRP laminate with 0.25 mm ply thickness at 4.0 mm transverse crack spacing and an applied laminate stress 0.2 GPa. The maximum crack opening displacement of the parabolic solution of the damage variables was higher than that of the infinite series solution. Therefore, the parabolic crack opening assumption and loosening of the boundary condition (Eqs. (67) and (68)) contributed to improving the crack opening displacement. The high crack opening displacement results in a large rate of stiffness reduction; therefore, this assumption contributes to the analytical accuracy of stiffness reduction, as well as the simplification of the damage variable form.

The effective thermal expansion coefficient of the $[0_2/90_2]_s$ CFRP laminate with a ply thickness of 0.125 mm was calculated and compared with experimental results [41]. The material parameters of CFRP2 were used for calculation. Figure 5 shows the predicted effective thermal expansion coefficients. By assuming the parabolic opening displacement and loosening the boundary conditions, the parabolic solution results were closer to the experimental results than the infinite series solution results. The result is clear from the fact that the crack opening displacement of the parabolic solution is higher than that of infinite series solution. The thermal stress of a ply in composite laminate is induced as temperature changes due to mismatch in the thermal expansion coefficients between plies with different orientations [41,42]. The large crack opening of the damaged 90° ply results in low effective ply stiffness. Therefore, the load bearing capacity of the 90° ply is reduced, and the thermal stress in the 0° layers becomes large. As a result, the effective laminate thermal expansion coefficient approaches the thermal expansion coefficient of 0° plies that have low thermal expansion coefficient.

However, the parabolic solution results are slightly higher than the experimental results at high crack density because of the assumption that the neighboring ply is rigid.

3.2 Angle-ply laminate

Unlike conventional shear-lag analyses, the present model uses the three-dimensional laminate theory; therefore, all effective thermoelastic properties of composite laminates with various layups can be determined. Figure 6 shows the effective Young's moduli, shear moduli, Poisson's ratios, and thermal expansion coefficients of the angle-ply $[55/-55]_s$ GFRP laminate with a 0.203 mm ply thickness, where the material parameters of GFRP1 were used for calculations. The FEA results [35] are plotted for comparison. Thus, the present model with a parabolic solution can reproduce the change in all effective thermoelastic properties due to transverse cracking. The effective laminate Young's modulus E_Z^L in the thickness direction is slightly reduced due to Poisson's effect.

Figure 7 depicts the normalized effective axial Young's modulus of the $[0/\theta/0]$ (θ = 90°, 60°, 45°) CFRP laminate based on the present and experimental results [43] to verify the present model for cracking in off-axis plies. The material parameter CFRP3 was used, and the ply thickness was 0.15 mm. The laminate layups were $[0/90_8/0]_s$, $[0/60_8/0]_s$, and $[0/45_8/0]_s$. The present model quantitatively agrees with the experimental results regardless of the fiber angle in the middle plies. Therefore, the proposed model can be applied to express the effective mechanical properties of cracked composite laminates in structural components subjected to multiaxial loading.

3.3 Quasi-isotropic laminate

Quasi-isotropic laminates develop transverse cracks in multiple ply orientations. Tong et al. [44] examined the cracks in the $[0/90/-45/45]_s$ GFRP laminate with a 0.5 mm ply thickness. In Tong's experiments, the cracks in the 90° plies traversed the width and thickness of the 90° plies, while the cracks did not fully propagate in the 45° and -45° plies. Singh and Talreja [45] defined the relative density factor ρ_r as the ratio of the actual surface area for partial cracks to the surface area for full cracks is defined as follows:

$$\rho_r = \frac{\text{Actual surface area for partial cracks}}{\text{Surface area for full cracks}}. \tag{80}$$

By introducing ρ_r, the crack density is defined as the sum of crack area contained per volume of the damaged ply. It means that a one large crack is equivalent to two small cracks with same crack surface area of the one large crack. The relative density factor could not be calculated using the data from Tong's experiments. Therefore, the transverse crack density in -45° and 45° plies was assumed to be a 90° transverse crack density multiplied a relative density factor ρ_r. Three values of ρ_r were considered: 0.25, 0.5, and 1. Figure 8 shows the normalized axial Young's modulus and in-plane Poisson's ratio of the quasi-isotropic GFRP laminate as functions of 90° transverse crack density, as

predicted by the proposed model using the material parameters of GFRP2, as well as the experiments of Tong et al. [44]. The present model with $\rho_r = 0.5$ is in the best agreement with the experimental results, which is consistent with the study of Singh and Talreja [45]. The results indicate that the present model can quantitatively predict the stiffness reduction of cracked composite laminate with arbitrary layups.

The three-dimensional stiffness reduction model for composite laminates containing transverse cracks is formulated, and thermomechanical properties of damaged composite laminate is predicted as a function of transverse crack density. To discuss crack growth in each layer of laminates with arbitrary layups, formulation of a crack growth analysis method using stress and energy criteria is a future task.

4 Conclusion

In this study, a three-dimensional effective compliance model is developed for composite laminates with transverse cracking. Three-dimensional laminate theory is used to reproduce all the thermoelastic properties of damaged laminates with various layups. Lopes' effective compliance [36] of the damaged ply is used to represent the stiffness degradation due to transverse cracking based on CDM. The damage variable d_2 is formulated based on a three-dimensional micromechanical model, where the boundary conditions are loosened and parabolic crack opening is assumed.

The effective thermomechanical properties of various composite laminates are predicted using the proposed model with both infinite series and simple parabolic solutions and compared with FEA and experimental results. The parabolic solution results showed better agreement with the FEA and experimental results than the infinite series solution, regardless of the laminate layup configuration. Therefore, this assumption contributes to the analytical accuracy of the stiffness reduction prediction while simplifying calculation of the damage variable.

Acknowledgement

This research was supported by the Council for Science, Technology, and Innovation (CSTI) and the Cross-Ministerial Strategic Innovation Promotion Program (SIP), "Materials Integration for Revolutionary Design System of Structural Materials" (Funding agency: JST). S.O. appreciates the support from JSPS KAKENHI Grant No. JP 22K14150.

Declaration of conflicting interests

The authors declare that there is no conflict of interest.

References

[1] Cox HL. The elasticity and strength of paper and other fibrous materials. Br J Appl Phys.

1952;3:72–79.

[2] Garrett KW, Bailey JE. Multiple transverse fracture in 90º cross-ply laminates of a glass fibre-reinforced polyester. J Mater Sci [Internet]. 1977;12:157–168. Available from: http://link.springer.com/10.1007/BF00738481.

[3] Highsmith AL, Reifsnider KL. Stiffness-Reduction Mechanisms in composite Laminates. In: Reifsnider KL, editor. Damage Compos Mater basic Mech accumulation, Toler Charact. Philadelphia: ASTM; 1982. p. 103–117.

[4] Manders PW, Chou T-W, Jones FR, et al. Statistical analysis of multiple fracture in 0º/90º/0º glass fibre/epoxy resin laminates. J Mater Sci [Internet]. 1983;18:2876–2889. Available from: http://link.springer.com/10.1007/BF00700768.

[5] Fukunaga H, Chou T-W, Peters PWM, et al. Probabilistic Failure Strength Analyses of Graphite/Epoxy Cross-Ply Laminates. J Compos Mater [Internet]. 1984;18:339–356. Available from: http://journals.sagepub.com/doi/10.1177/002199838401800403.

[6] Ogin SL, Smith PA, Beaumont PWR. Matrix cracking and stiffness reduction during the fatigue of a (0/90)s GFRP laminate. Compos Sci Technol [Internet]. 1985;22:23–31. Available from: https://linkinghub.elsevier.com/retrieve/pii/0266353885900880.

[7] Ogin SL, Smith PA, Beaumont PWR. A stress intensity factor approach to the fatigue growth of transverse ply cracks. Compos Sci Technol [Internet]. 1985;24:47–59. Available from: https://linkinghub.elsevier.com/retrieve/pii/0266353885900600.

[8] Nuismer RJ, Tan SC. Constitutive Relations of a Cracked Composite Lamina. J Compos Mater. 1988;22:306–321.

[9] Laws N, Dvorak GJ. Progressive Transverse Cracking In Composite Laminates. J Compos Mater [Internet]. 1988;22:900–916. Available from: http://journals.sagepub.com/doi/10.1177/002199838802201001.

[10] Tan SC, Nuismer RJ. A Theory for Progressive Matrix Cracking in Composite Laminates. J Compos Mater. 1989;23:1029–1047.

[11] Lim SG, Hong CS. Prediction of Transverse Cracking and Stiffness Reduction in Cross-Ply Laminated Composites. J Compos Mater [Internet]. 1989;23:695–713. Available from: http://journals.sagepub.com/doi/10.1177/002199838902300704.

[12] Flaggs DL. Prediction of Tensile Matrix Failure in Composite Laminates. J Compos Mater. 1985;19:29–50.

[13] Lee JW, Daniel IM. Progressive Transverse Cracking of Crossply Composite Laminates. J Compos Mater. 1990;24:1225–1243.

[14] Berthelot J-M, Leblond P, El Mahi A, et al. Transverse cracking of cross-ply laminates: Part 1. Analysis. Compos Part A Appl Sci Manuf [Internet]. 1996;27:989–1001. Available from: https://linkinghub.elsevier.com/retrieve/pii/1359835X9680002A.

[15] Hashin Z. Analysis of Orthogonally Cracked Laminates Under Tension. J Appl Mech. 1987;54:872–879.

[16] Hashin Z. Analysis of stiffness reduction of cracked cross-ply laminates. Eng Fract Mech. 1986;25:771–778.

[17] Lee J-W, Allen DH, Harris CE. Internal State Variable Approach for Predicting Stiffness Reductions in Fibrous Laminated Composites with Matrix Cracks. J Compos Mater [Internet]. 1989;23:1273–1291. Available from: http://journals.sagepub.com/doi/10.1177/002199838902301205.

[18] Hajikazemi M, McCartney LN, Van Paepegem W, et al. Theory of variational stress transfer in general symmetric composite laminates containing non-uniformly spaced ply cracks. Compos Part A Appl Sci Manuf [Internet]. 2018;107:374–386. Available from: https://linkinghub.elsevier.com/retrieve/pii/S1359835X18300216.

[19] Hajikazemi M, McCartney LN, Van Paepegem W. Matrix cracking initiation, propagation and laminate failure in multiple plies of general symmetric composite laminates. Compos Part A Appl Sci Manuf [Internet]. 2020;136:105963. Available from: https://doi.org/10.1016/j.compositesa.2020.105963.

[20] Vinogradov V, Hashin Z. Variational analysis of cracked angle-ply laminates. Compos Sci Technol. 2010;70:638–646.

[21] Vinogradov V. A variational method for analysis of laminates with parallel arrays of intralaminar cracks. Int J Numer Methods Eng [Internet]. 2019;120:666–705. Available from: http://doi.wiley.com/10.1002/nme.6152.

[22] Kachanov LM. Time of the Rupture Process under Creep Conditions. Izv Akad Nauk SSSR, Otd Teckhnicheskikh Nauk. 1958;8:26–31.

[23] Allen DH, Harris CE, Groves SE. A thermomechanical constitutive theory for elastic composites with distributed damage—I. Theoretical development. Int J Solids Struct [Internet]. 1987;23:1301–1318. Available from: https://linkinghub.elsevier.com/retrieve/pii/0020768387901077.

[24] Talreja R. A Continuum Mechanics Characterization of Damage in Composite Materials. Proc R Soc A Math Phys Eng Sci. 1985;399:195–216.

[25] Kitagawa Y, Arai M, Yoshimura A, et al. Prediction of transverse crack multiplication of CFRP cross-ply laminates under tension-tension fatigue load. Adv Compos Mater [Internet]. 2022;00:1–18. Available from: https://doi.org/10.1080/09243046.2022.2113700.

[26] Aoki R, Higuchi R, Yokozeki T. Fatigue simulation for progressive damage in CFRP laminates using intra-laminar and inter-laminar fatigue damage models. Int J Fatigue [Internet]. 2021;143:106015. Available from: https://doi.org/10.1016/j.ijfatigue.2020.106015.

[27] Bhattacharyya R, Basu PK. Multiscale crack band model for eigenstrain based reduced order

homogenization. Comput Mech [Internet]. 2020;66:1237–1255. Available from: https://doi.org/10.1007/s00466-020-01896-0.

[28] Sun Z, Li C, Tie Y. Experimental and numerical investigations on damage accumulation and energy dissipation of patch-repaired CFRP laminates under repeated impacts. Mater Des [Internet]. 2021;202:109540. Available from: https://doi.org/10.1016/j.matdes.2021.109540.

[29] Bhattacharyya R, Basu PK. Multiscale progressive damage analysis of CFRP composites using a mechanics based constitutive relation. Compos Struct [Internet]. 2020;235:111759. Available from: https://doi.org/10.1016/j.compstruct.2019.111759.

[30] Okabe T, Onodera S, Kumagai Y, et al. Continuum damage mechanics modeling of composite laminates including transverse cracks. Int J Damage Mech [Internet]. 2018;27:877–895. Available from: http://journals.sagepub.com/doi/10.1177/1056789517711238.

[31] Onodera S, Okabe T. Three-dimensional analytical model for effective elastic constants of transversely isotropic plates with multiple cracks: Application to stiffness reduction and steady-state cracking of composite laminates. Eng Fract Mech [Internet]. 2019;219:106595. Available from: https://linkinghub.elsevier.com/retrieve/pii/S001379441930462X.

[32] Onodera S, Okabe T. Analytical model for determining effective stiffness and mechanical behavior of polymer matrix composite laminates using continuum damage mechanics. Int J Damage Mech [Internet]. 2020;29:1512–1542. Available from: http://journals.sagepub.com/doi/10.1177/1056789520939624.

[33] Nagumo Y, Onodera S, Okabe T. Prediction of transverse crack progression based on continuum damage mechanics and its application to composite laminates and filament-wound cylindrical pressure vessels. Adv Compos Mater [Internet]. 2022;00:1–17. Available from: https://doi.org/10.1080/09243046.2022.2048452.

[34] Li S, Wang M, Jeanmeure L, et al. Damage related material constants in continuum damage mechanics for unidirectional composites with matrix cracks. Int J Damage Mech [Internet]. 2019;28:690–707. Available from: http://journals.sagepub.com/doi/10.1177/1056789518783239.

[35] Gudmundson P, Zang W. An analytic model for thermoelastic properties of composite laminates containing transverse matrix cracks. Int J Solids Struct. 1993;30:3211–3231.

[36] Lopes CS, Camanho PP, Gürdal Z, et al. Low-velocity impact damage on dispersed stacking sequence laminates. Part II: Numerical simulations. Compos Sci Technol [Internet]. 2009;69:937–947. Available from: http://dx.doi.org/10.1016/j.compscitech.2009.02.015.

[37] McCartney LN. Theory of stress transfer in a 0°—90°—0° cross-ply laminate containing a parallel array of transverse cracks. J Mech Phys Solids [Internet]. 1992;40:27–68. Available from: https://linkinghub.elsevier.com/retrieve/pii/002250969290226R.

[38] Murakami S. Continuum Damage Mechanics. Solid Mech. its Appl. Dordrecht: Springer Netherlands; 2012.

[39] McCartney L, Schoeppner GA, Becker W. Comparison of models for transverse ply cracks in composite laminates. Compos Sci Technol [Internet]. 2000;60:2347–2359. Available from: https://linkinghub.elsevier.com/retrieve/pii/S0266353800000300.

[40] McCartney L, Schoeppner GA. Predicting the effect of non-uniform ply cracking on the thermoelastic properties of cross-ply laminates. Compos Sci Technol [Internet]. 2002;62:1841–1856. Available from: https://linkinghub.elsevier.com/retrieve/pii/S026635380200091X.

[41] Kim RY, Crasto AS, Schoeppner GA. Dimensional stability of composite in a space thermal environment. Compos Sci Technol. 2000;60:2601–2608.

[42] Kobayashi S, Shimpo T, Goto K. Microscopic damage behavior in carbon fiber reinforced plastic laminates for a high accuracy antenna in a satellite under cyclic thermal loading. Adv Compos Mater [Internet]. 2019;28:259–269. Available from: https://doi.org/10.1080/09243046.2018.1551745.

[43] Fikry MJM, Ogihara S, Vinogradov V. The effect of matrix cracking on mechanical properties in FRP laminates. Mech Adv Mater Mod Process [Internet]. 2018;4:3. Available from: https://link.springer.com/10.1186/s40759-018-0036-6.

[44] Tong J, Guild FJ, Ogin SL, et al. On matrix crack growth in quasi-isotropic laminates—I. Experimental investigation. Compos Sci Technol [Internet]. 1997;57:1527–1535. Available from: https://linkinghub.elsevier.com/retrieve/pii/S0266353897000808.

[45] Singh CV, Talreja R. A synergistic damage mechanics approach for composite laminates with matrix cracks in multiple orientations. Mech Mater [Internet]. 2009;41:954–968. Available from: http://dx.doi.org/10.1016/j.mechmat.2009.02.008.

[46] Tong J, Guild FJ, Ogin SL, et al. On matrix crack growth in quasi-isotropic laminates - II. Finite element analysis. Compos Sci Technol. 1997;

Words count: 5690 words

Tables and Figures

Table 1 Material properties of CFRP and GFRP plies.

Material	Fig. No.	E_1 (GPa)	E_2 (GPa)	G_{12} (GPa)	G_{23} (GPa)	ν_{12}	ν_{23}	α_1 (10^{-6}/deg.)	α_2 (10^{-6}/deg.)
CFRP1 [39,40]	Figs. 3 & 4	144.78	9.58	4.785	3.090	0.31	0.55	-	-
CFRP2 [21,41]	Fig. 5	138	10.3	5.5	3.6	0.3	0.43	0.43	25.8
GFRP1 [35]	Fig. 6	41.7	13	3.4	4.58	0.3	0.42	6.72	29.3
CFRP3 [43]	Fig. 7	135	8.5	4.8	2.7	0.34	0.49	-	-
GFRP2 [46]	Fig. 8	46	13	5	4.6	0.3	0.42	-	-

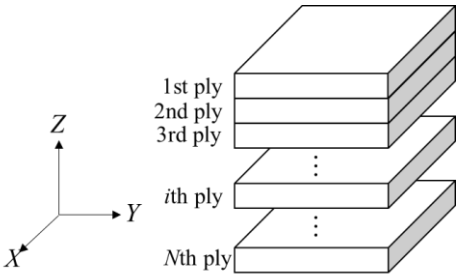

Figure 1 A laminate formulated by stacking plies in the *Z*-direction, where the coordinates (*X*, *Y*, *Z*) represent the laminate coordinate system.

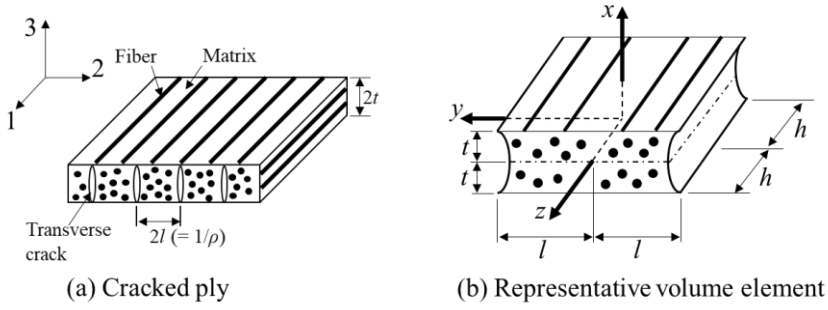

(a) Cracked ply (b) Representative volume element

Figure 2 (a) A ply with transverse cracks and (b) RVE of the damaged ply; (1, 2, 3) is the material coordinate system, while (*x*, *y*, *z*) is the RVE coordinate system.

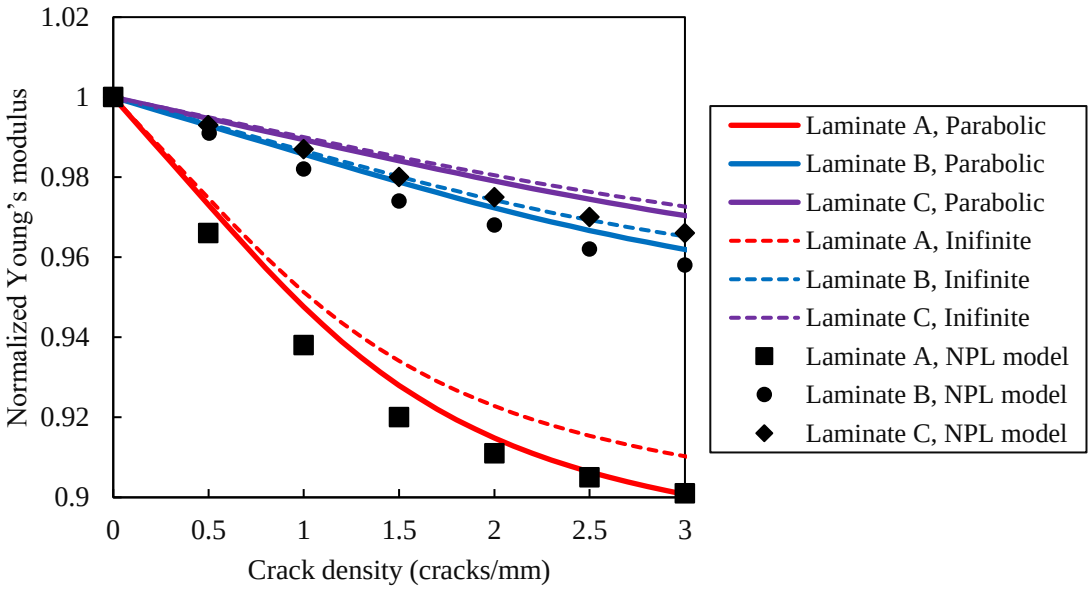

Figure 3 Nominal axial Young's modulus of cross-ply CFRP laminates as a function of transverse crack density. Layups of Laminate A, B, and C are $[0/90_2]_s$, $[0/90_2/0]_s$, and $[0/90/0/90]_s$, respectively. Results shown are from the present stiffness reduction model with parabolic and infinite series solutions and NPL model [40].

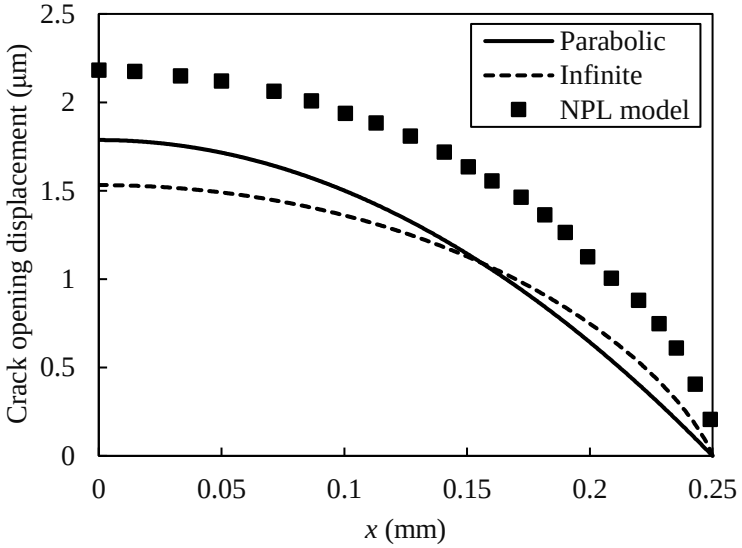

Figure 4 Crack opening displacement of a transverse crack in $[0/90]_s$ CFRP laminate with transverse crack spacing of 4.0 mm at applied laminate stress of 0.2 GPa. Results shown are from the present stiffness reduction model with parabolic and infinite series solutions and NPL model [39].

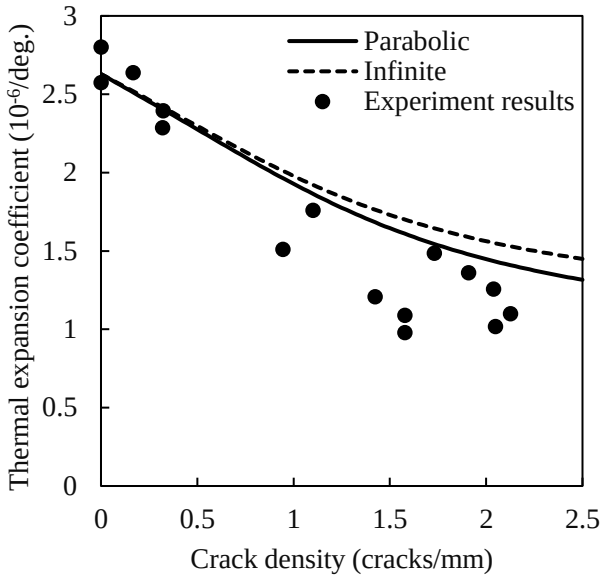

Figure 5 Thermal expansion coefficient as a function of transverse crack density of $[0_2/90_2]_s$ CFRP laminate with surface cracking. Results shown are from the present stiffness reduction model with parabolic and infinite series solutions and the experimental results of Tong et al. [41].

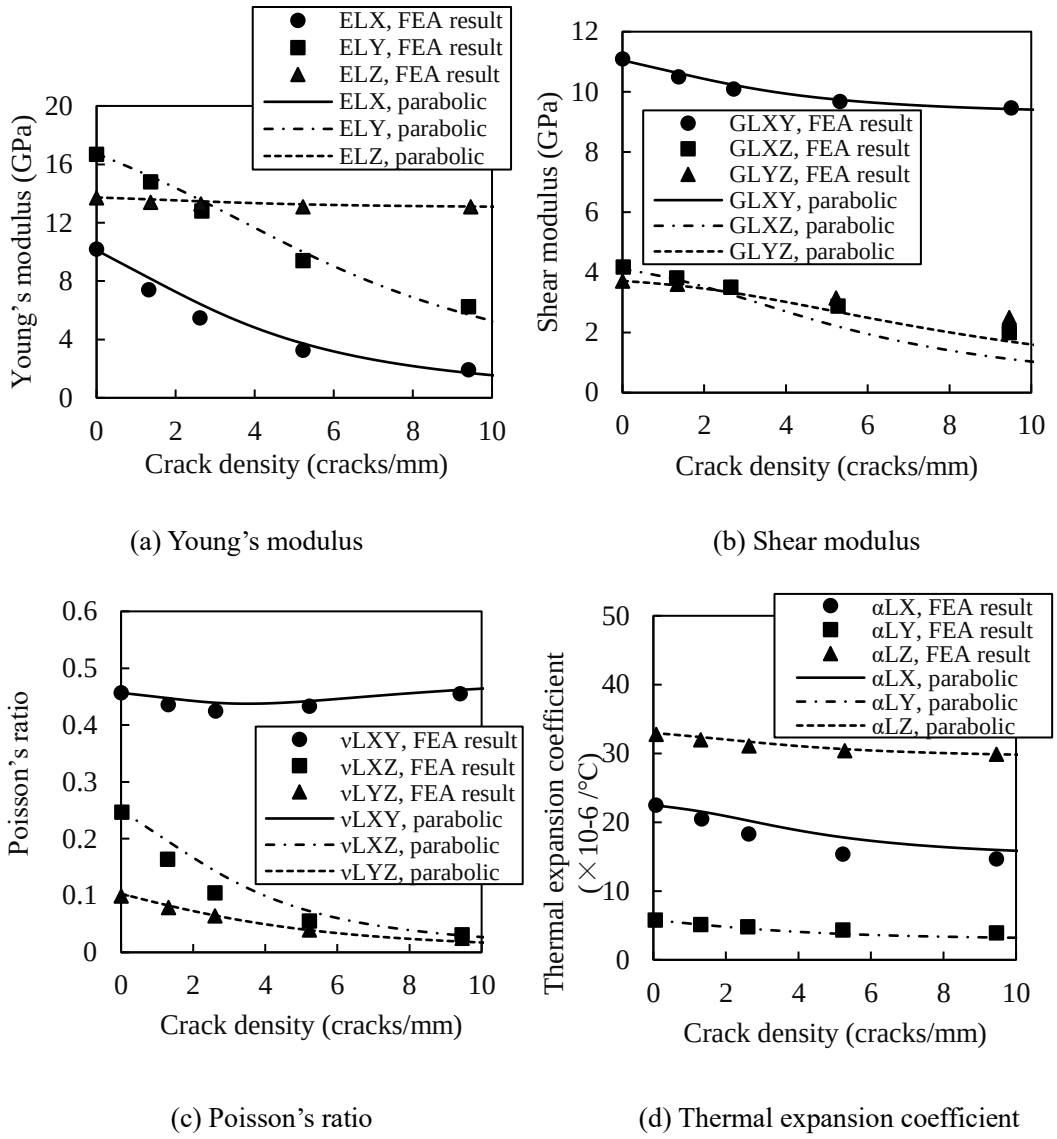

Figure 6 (a) Young's moduli, (b) shear moduli, (c) Poisson's ratios, and (d) thermal expansion coefficients as a function of transverse crack density of $[55/-55]_s$ angle-ply GFRP laminate. FEA results [35] are plotted for comparison.

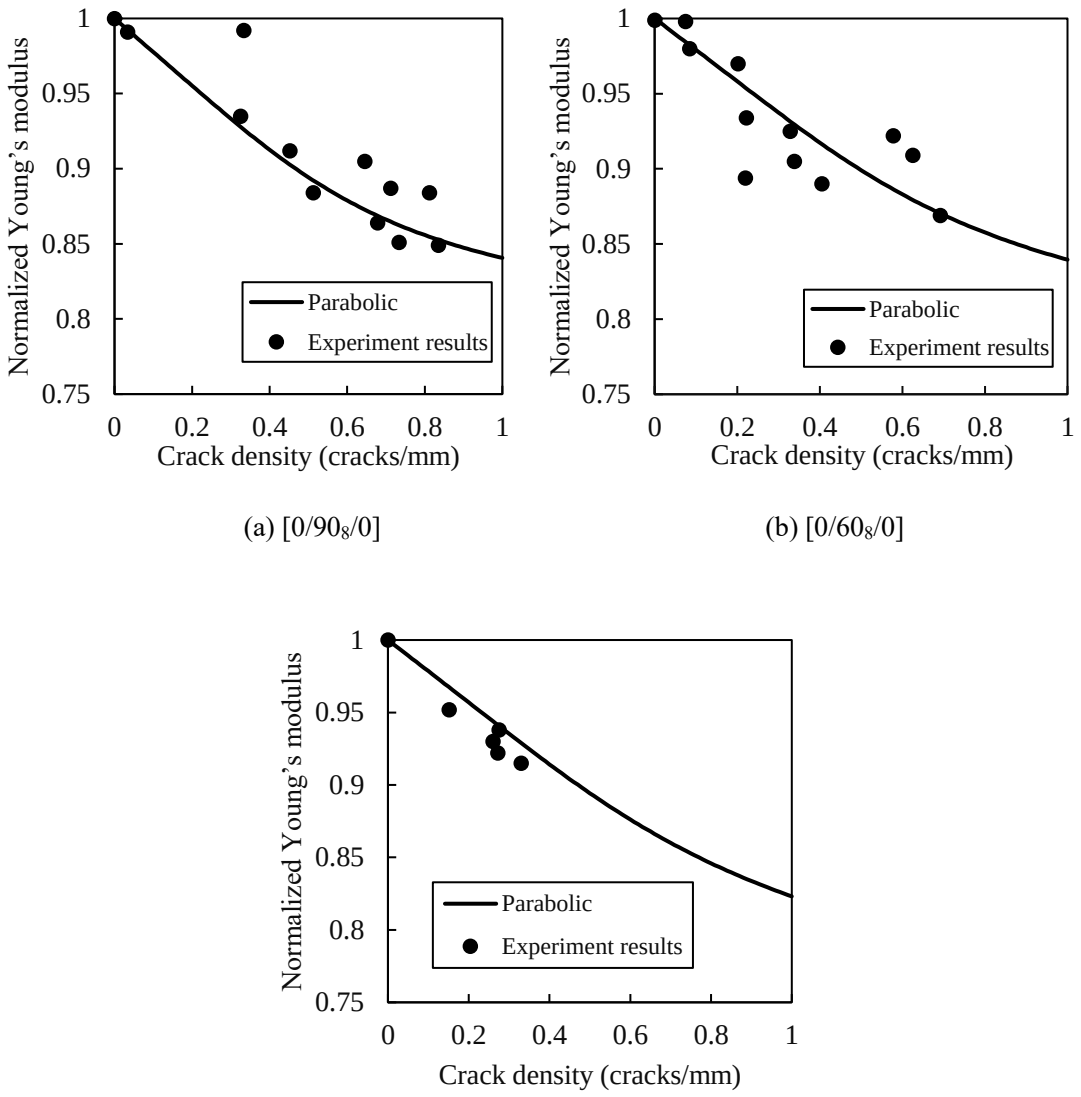

(a) $[0/90_8/0]$ (b) $[0/60_8/0]$

(c) $[0/45_8/0]$

Figure 7 Normalized axial Young's modulus of (a) $[0/90_8/0]$, (b) $[0/60_8/0]$, and (c) $[0/45_8/0]$ CFRP laminates as a function of transverse crack density. Experiment results [43] are plotted for comparison.

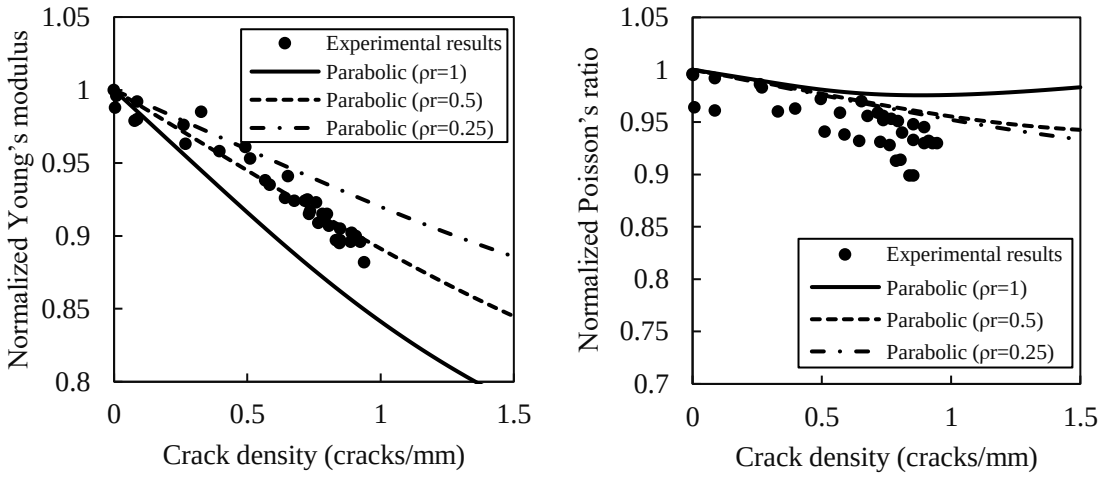

(a) Young's modulus (b) Poisson's ratio

Figure 8 (a) Normalized axial Young's modulus and (b) normalized in-plane Poisson ratio of $[0/90/-45/45]_s$ quasi-isotropic GFRP laminate as a function of 90° transverse crack density. Experimental results [44] are plotted for comparison.